Heliyon 10 (2024) e27182

Contents lists available at ScienceDirect

Heliyon

journal homepage: www.cell.com/heliyon

Research article

Biocidal effects of organometallic materials supported on ZSM-5 Zeolite: Influence of the physicochemical and surface properties

I. Huenuvil-Pacheco [a,b], A.F. Jaramillo [c,d,**], N.J. Abreu [a,e,*], K. Garrido-Miranda [f,g], G. Sánchez-Sanhueza [h], G. González-Rocha [i], C. Medina [j], L.F. Montoya [b], J.P. Sanhueza [k], M.F. Melendrez [l]

[a] *Departamento de Ingeniería Química, Facultad de Ingeniería y Ciencias, Universidad de La Frontera, 01145 Francisco Salazar, Temuco 4780000, Chile*
[b] *Department of Chemical Engineering, University of Concepción, Concepción 4070386, Chile*
[c] *Department of Mechanical Engineering, Universidad de La Frontera, 01145 Francisco Salazar, Temuco 4780000, Chile*
[d] *Departamento de Ingeniería Mecánica, Universidad de Córdoba, Cr 6 #76-103, Montería 230002, Colombia*
[e] *Centro de Manejo de Residuos y Bioenergía, BIOREN, Universidad de La Frontera, 01145 Francisco Salazar, Temuco 4780000, Chile*
[f] *Agriaquaculture Nutritional Genomic Center (CGNA), Temuco 4780000, Chile*
[g] *Núcleo de Investigación en Bioproductos y Materiales Avanzados (BIOMA), Universidad Católica de Temuco, Avenida Rudecindo Ortega 02950, Campus San Juan Pablo II, Temuco 4780000, Chile*
[h] *Department of Restorative Dentistry, Faculty of Dentistry, Universidad de Concepción, 1550 Roosevelt St, Concepcion 4030000, Chile*
[i] *Laboratorio de Investigación en Agentes Antibacterianos, Departamento de Microbiología, Facultad de Ciencias Biológicas, Universidad de Concepción, Concepción 4030000, P.O. Box C-160, Chile*
[j] *Department of Mechanical Engineering (DIM), Faculty of Engineering, University of Concepción, Edmundo Larenas 219, Concepcion 4070409, Chile*
[k] *Department of Materials Engineering (DIMAT), Faculty of Engineering, Universidad de Concepción, 315 Edmundo Larenas, Concepcion, 4070415, Chile*
[l] *Facultad de Ciencias para el Cuidado de la Salud, Universidad San Sebastían, Campus Las Tres Pascualas, Lientur 1457, Concepción, 4060000, Chile*

ARTICLE INFO

Keywords:
ZSM-5 zeolite
Organo-metallic biocide
Capsaicin
Copper oxide nanoparticles
Biofouling

ABSTRACT

Antifouling coatings containing biocidal agents can be used to prevent the accumulation of biotic deposits on submerged surfaces; however, several commercial biocides can negatively affect the ecosystem. In this study, various formulations of a potential biocide product comprising copper nanoparticles and capsaicin supported on zeolite ZSM-5 were analyzed to determine the influence of the concentration of each component. The incorporation of copper was evidenced by scanning electron microscopy and energy dispersive spectroscopy. Similarly, Fourier-transform infrared spectroscopy confirmed that capsaicin was supported on the zeolite surface. The presence of capsaicin on the external zeolite surface significantly reduced the surface area of the zeolite. Finally, bacterial growth inhibition analysis showed that copper nanoparticles inhibited the growth of strains *Idiomarina loihiensis* UCO25, *Pseudoalteromonas* sp. UCO92, and *Halomonas boliviensis* UCO24 while the organic component acted as a reinforcing biocide.

* Corresponding author. Universidad de Córdoba, Cr 6 #76-103, Montería 230002, Colombia.
** Corresponding author. Universidad de La Frontera, 01145 Francisco Salazar, Temuco 4780000, Chile.
E-mail addresses: norberto.abreu@ufrontera.cl (A.F. Jaramillo), andresjaramillom@correo.unicordoba.edu.co, andresfelipe.jaramillo@ufrontera.cl (N.J. Abreu).

https://doi.org/10.1016/j.heliyon.2024.e27182
Received 24 October 2023; Received in revised form 23 February 2024; Accepted 26 February 2024
Available online 27 February 2024

1. Introduction

Marine biofouling is an unwanted adherence phenomenon that results in the accumulation of biotic deposits on artificial surfaces submerged in or in contact with seawater [1,2]. Biofouling is a complex phenomenon that involves several species ranging from microorganisms such bacteria to invertebrates [3] and typically consists of two main stages: micro- and macro-fouling [4]. During the first stage, bacteria begin to adhere to the surface, forming a microfouling biofilm. During the subsequent macrofouling stage, larger organisms such as algae and invertebrates adhere to the surface [5].

Biofouling affects several economic spheres; for instance, biofouling gradually increases the fuel consumption of fishing vessels owing to increased drag resistance and accelerates the corrosion of maritime infrastructure [3,6]. In aquaculture, biofouling restricts the opening of nets, significantly increasing their weight and hindering the elimination of waste products [7,8]. Similarly, the adhesion of marine species to the surface of boats could result the transport of exotic species, including invasive organisms, to environments other than their natural habitats, thereby negatively impacting native biodiversity [9]. Antifouling coatings can be applied to a surface to inhibit the growth rate of organisms [2,10,11]; however, these coatings can damage marine microbiota, flora and fauna, particularly when they contain biocides with high toxicity against target and non-target organisms, and thus threaten to ecological systems [12, 13]. Thus, the design of materials that employ environmentally friendly biocides in place of conventional biocides is of great importance to the scientific community [6,14].

Antifouling coatings are commonly contain inorganic, organometallic, or organic biocidal agents [15]. Most commercially available antifouling products contain copper oxides (CuO and Cu_2O), silicon oxide (SiO_2), zinc (Zn), and titanium oxide (TiO_2) as the main compounds [16]. They may also contain organic compounds that mitigate the toxic effects of metal oxides on organisms that do not contribute to biofouling [17]. Copper nanomaterials have become important biocidal agents owing to their high effectiveness in inhibiting inlay formation [15,18], which results from the ability of copper ions to destroy the outer cell membranes of microorganisms [19,20].

Moreover, the addition of an organic agent can reinforce the biocidal effect, thereby affording greater control over the adhesion of encrusting organisms [15,17]. Capsaicin, an amide alkaloid with pH-sensitive antibacterial and antiinlay properties, is commonly used to formulate such functional coatings [14,21,22]. However, directly introducing biocidal materials in the formulation of the coating results in a small contact area between the biocide and the microorganism contact area is low, along with uncontrolled release of the biocide into the marine environment, thereby limiting the duration of the required effect. Depositing biocidal materials on a support matrix is therefore necessary to increase the contact surface area and retention of biocidal agents, thus regulating their release into the marine environment [23].

In this way, the active compounds (organic, inorganic, and organometallic) can be incorporated on the surface of supports, such as zeolites or other microporous materials. The large surface area increases the availability of copper and capsaicin ions within pores and promotes the interaction between the biocide and biofilm, thereby maintaining the biocidal effect over time [24]. Zeolites are micro- and mesoporous alkaline earth metal aluminosilicates with tetrahedral $[SiO_4]^{4-}$ and $[AlO_4]^{5-}$ networks interconnected by oxygen atoms. This porous network is sufficiently large to contain extra structural cations within its many molecular scale cavities and channels, allowing the zeolite material to adsorb molecules ranging in size from diatomic hydrogen to organic compounds measuring of several nanometers [25,26]. Similarly, the chemical structure of zeolites and the electronegativity imposed by the aluminates allow the incorporation of compensation cations such as transition metal cations through physical and thermochemical transformations [25, 27].

Owing to these properties, along with their high mechanical and thermal stabilities, zeolites have several applications as adsorbents, catalysts, ion exchange matrices, antimicrobial materials, and filter media [28,29]. Specifically, ZSM-5 zeolite is a shape-selective material with uniformly sized pores and has shown excellent results in supporting metals and some organic molecules, enhancing their controlled delivery [30,31]. The three-dimensional network of channels and cages present in ZSM-5 zeolite could favor the controlled diffusion of copper within the zeolite pores. The ionic exchange properties could allow the incorporation of copper nanoparticles, which act as stabilizers in the zeolite structure. On the other hand, preliminary works have shown that this zeolite presents some pores with a higher size, even some mesopores where the capsaicin molecule could be allocated, thus allowing the combined action of both biocidal agents and enhancing their availability and contact surface [32–34].

2. Materials and methods

Synthetic ZSM-5 (840NHA) zeolite with compensating NH^{4+} cations was purchased from TOSOH (Ohio, USA). Copper nitrate trihydrate ($Cu[NO_3]_2{\cdot}3H_2O$) (99.9% purity) and ethanol (C_2H_6O) (purity $\geq$99.5%) were supplied by Merck S.A (Darmstadt, Germany). Natural capsaicin (99.5 purity) was obtained from Penta Manufacturing (Livingston, NJ, USA).

The following reagents were used in the antifouling assays: Marine Agar 2216/Marine Broth 2216 (BD Difco™ Detroit, USA); halophilic bacteria including *Idiomarina loihiensis* UCO25; *Pseudoalteromonas* sp. UCO92*; Halomonas boliviensis* UCO24, isolated from seawater in the Pacific Ocean of southern hemisphere. Analytically pure barium chloride ($BaCl_2$) and sulfuric acid (H_2SO_4) with analytic purity were purchased from Sigma Aldrich (Missouri, USA). A solution of sodium chloride in sterile water (0.9% w/v) was obtained from Fresenius Kabi (Bad Homburg, Germany).

2.1. Materials synthesis

Cu particles and capsaicin were incorporated into the synthesized zeolite via consecutive metal exchange and organic modification procedures, respectively. Each of these processes is described in detail below.

2.1.1. Impregnation of copper particles into the Zeolite

The ZSM-5 zeolite (Z40) was impregnated with copper particles within the pores and on its outer surface using a wet impregnation method. The copper precursor copper nitrate trihydrate was dissolved in deionized water. The solution volume was determined at a ratio of 10 cm^3 of copper solution to 1 g of zeolite. The concentration of this copper nitrate solution was determined to obtain a nominal copper content (Cu %) of 2%, 4%, and 8%, as calculated using Equation No 1:

$$\text{Cu } \% = \frac{\text{w}_{\text{Cu}}\ (\text{g})}{\text{w}_{\text{Cu}}\ (\text{g}) + \text{w}_{\text{Z40}}\ (\text{g})} \tag{1}$$

Where w_{Cu} is the relative mass of the copper atom within the ($Cu[NO_3]_2{\cdot}3H_2O$) molecule and w_{Z40} is the mass of the ZSM-5 zeolite before modification. The zeolite was then suspended in the solution and continuously mixed under vacuum at 363 K in a temperature controlled rotatory evaporator (EV400H, LabTech). The samples were dried for 24 h at 373 K in an oven (WGLL-BE, FAITHFUL) and stored in a desiccator until use.

2.1.2. Zeolite modification by capsaicin diffusion and impregnation

Raw ZSM-5 and the Cu-modified zeolite samples (base zeolite) were impregnated with capsaicin using a capsaicin solution with a concentration determined such that a nominal capsaicin content (cps %) of 1% or 1.5% was obtained in the final zeolite sample, Equation No 2:

$$\text{Cps } \% = \frac{\text{w}_{\text{Cps}}(\text{g})}{\text{w}_{\text{cps}}\ (\text{g}) + \text{w}_{\text{base zeolite}}\ (\text{g})} \tag{2}$$

Where w_{cps} is the mass of the capsaicin molecule and $w_{base\ zeolite}$ is the mass of the base zeolite. The zeolite was suspended in the solution under continuous stirring for 24 h at 303 K in a closed flask in a temperature controlled rotatory evaporator (Biobase, China) to avoid capsaicin degradation and ensure the diffusion of capsaicin throughout the zeolite pore network. The excess solvent was removed subsequently under vacuum at 303 K using a rotatory evaporator. The modified samples were dried for 48 h at 303 K in an oven (WGLL-BE, FAITHFUL) and stored in a desiccator until further use. This method was designed to incorporate capsaicin on the external zeolite surface and encapsulate organic molecule within the zeolite pore system. The zeolite samples were labeled as Z40_Cuxxcpsyy, where "xx" refers to calculated Cu % and "yy" refers to calculated cps%.

2.2. Physicochemical characterization

2.2.1. Surface and textural properties

The textural properties of the generated materials were analyzed using nitrogen adsorption and desorption isotherms at 77 K using a NOVA 1000e analyzer (QuantaChrome, USA). The effect of modifying the surface characteristics was identified using the Brunauer-Emmett-Teller (BET) method. The pore size distribution was determined using the Horváth-Kawazoe (HK) method, and the volume of micropores and mesopores was determined using the Barrett-Joyner-Halenda (BJH) method. Samples for these tests were degassed at 303 K for 20 h to prevent capsaicin modification within the pores.

2.2.2. Scanning electron microscopy

The topography of the samples was analyzed via scanning electron microscopy (SEM) using an SU-3500 microscope (Hitachi, Japan) operated at 10.0 kV under high vacuum (30 Pa). Images were collected on a scale from 5 to 100 μm. Energy-dispersive spectroscopy (EDS) and electron microscopy verified the incorporation of copper nanoparticles into the zeolite structure.

2.2.3. X-ray diffraction

X-ray diffraction (XRD) patterns were acquired using a Bruker Endeavor D4/MAX-B diffractometer operated at 20 mA and 40 kV using a copper cathode lamp ($\lambda = 1541$ Å). The 2θ sweep was set from 4° to 80° in steps of 0.02° with a time interval of 1 s.

2.2.4. Surface characterization by Fourier transform infrared spectroscopy

Fourier-transform infrared (FTIR) spectra of the zeolite and capsaicin were acquired using a Cary 630 FTIR spectrometer (Agilent Technologies, Santa Clara, CA, USA). The analysis was performed in transmittance mode by obtaining 30 averaged spectra using the Attenuated Total Reflectance (ATR) sampling technique. The spectra were obtained in the range between 4000 and 500 cm^{-1}.

2.3. Bacterial growth inhibition study

The biocidal effects of the generated materials were analyzed using the Kirby-Bauer method. The marine bacteria *Idiomarina loihiensis* UCO25, *Pseudoalteromonas* sp. UCO92, and *Halomonas boliviensis* UCO24 were used to analyze the effect of biocidal materials

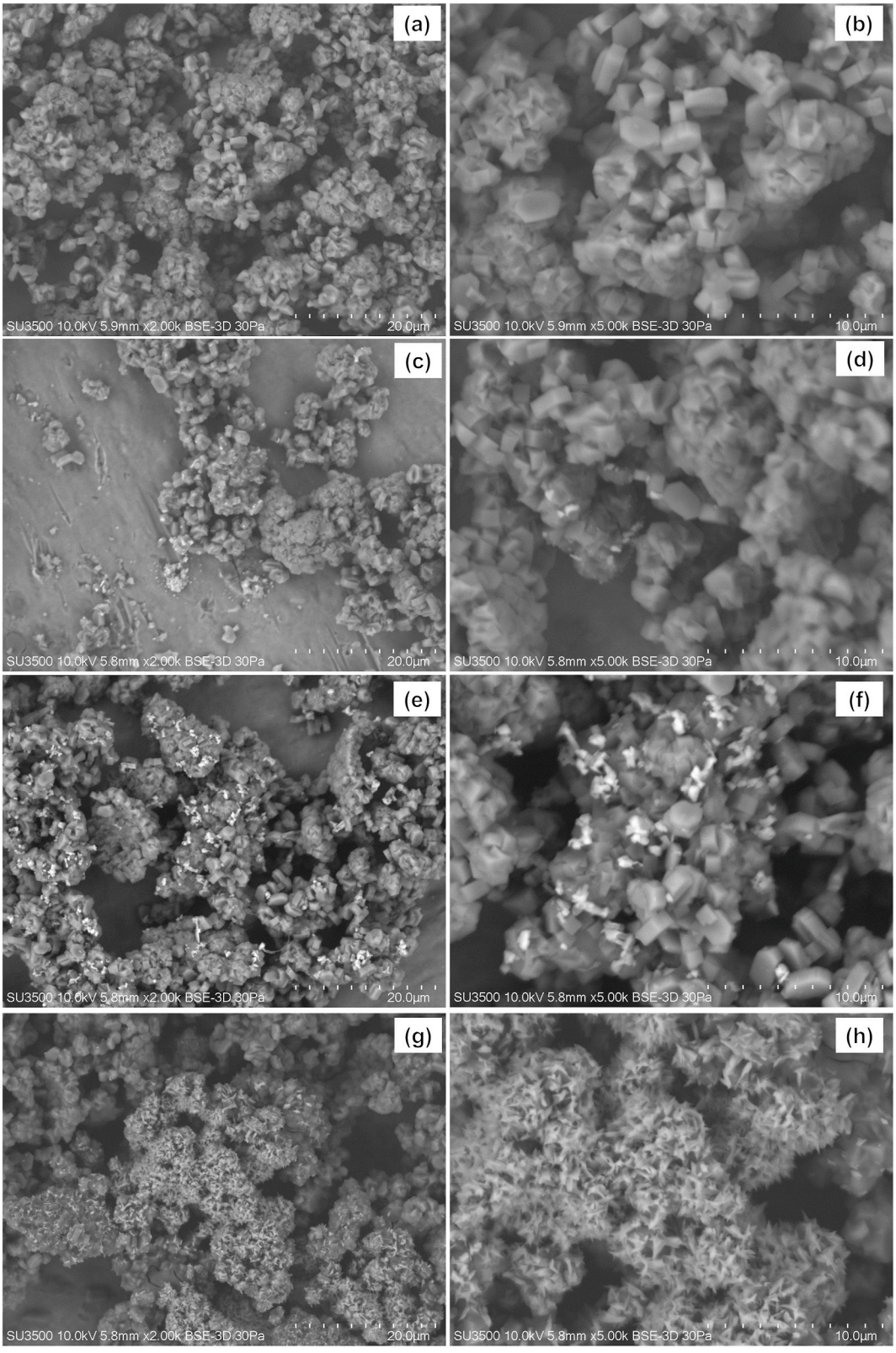

Fig. 1. SEM images of the zeolite samples before and after copper modification (a, b) Z40 (unmodified), (c, d) Z40Cu2, (e, f) Z40Cu4, (g, h) Z40Cu8.

against species commonly found to form microfouling films [35,36]. This method allows the determination of the sensitivity of a microorganism to a specific agent, and the absence or presence of an inhibitory area around the biocide material identifies its bacterial sensitivity [37].

Bacterial growth plates were prepared by initially culturing *I. loihiensis*, *Pseudoalteromonas* sp., and *H. boliviensis* strains on marine agar for 48 h. A bacterial colony was then transferred to marine broth and incubated for a further 48 h. The bacterial suspension was adjusted to a turbidity of 0.5 McFarland standard, equivalent to 1.5×10^8 CFU/mL. A 1/10 dilution was prepared, resulting in a final inoculum concentration of 1×10^7 CFU/mL. Pellets with diameters of 13 mm and thicknesses of 2 mm containing the biocidal materials (0.2 g) were prepared. Prior to each experiment, the pellets were sterilized under UV light for 20 min per side and deposited onto bacterial growth plates using alcohol-sterilized forceps. The tablets were deposited equidistant from each other at a distance of 24 mm from the center of the discs. The bacterial growth plates were then incubated for 48 h at 10 °C. Each sample was analyzed in triplicate. Statistical analysis of the samples was performed using Fisher's test of the least significant difference (LSD) from the inhibition halo formed, which determined the effects of the formulation at different concentrations of the biocides.

3. Results and discussion

3.1. Physicochemical and surface properties

The modified samples were analyzed to elucidate the effectiveness of the treatments and to evaluate their effects on the physicochemical and surface properties. Visual inspection of the samples after modification with different levels of copper revealed different tones (Fig. S1), which indicates the copper exchange occurred from the precursor solution to the zeolite samples. The intensity of the blue hue corresponded to the concentration of the precursor solution.

3.1.1. Scanning electron microscopy

The morphology of raw and modified ZSM-5 zeolites is depicted in Fig. 1. In this sense, SEM images with a 20 μm scale (Fig. 1 (a, c, e, g)) are presented to show the general morphology of the samples, and a magnification to 10 μm scale is also presented to depict the individual granules of zeolite (Fig. 1 (b, d, f, h)). SEM images of the raw zeolite (Fig. 1 (a)) revealed the presence of well-defined and uniform hexagonal platelet-shaped zeolite particles with a lamellar structure; individual granules with a mean diameter of 15 μm can also be observed (Fig. 1 (b)). Similar results were reported by previous studies using ZSM-5 zeolites [38,39]. Similarly, the presence of supported particles in the porous material (Fig. 1 (c, e, g)) provides clear evidence that the mineral retains its characteristic properties, suggesting that wet impregnation does not affect the external structure of the support. However, as the copper concentration increases, copper oxide particles seem to appear on the outer surface of the zeolite (Fig. 1 (d, f, h)). Moreover, in the samples with 8% copper loading (Fig. 1 (g, h)), the formation of larger copper oxide particles can be observed; these particles could be affecting the access to the microporous surface. In this sense, the use of copper concentrations higher than 8% could be unfavorable. Such results could also be attributed to the modification route applied. In this case, copper is not only added as a compensating cation, but bulk copper is also deposited within the porous structure, compromising the dispersion of particles and the surface area.

EDS analysis confirmed the presence of Cu in the modified zeolites. As expected, different Cu contents were observed in the samples, corresponding to the Cu concentration in the precursor solution. The EDS spectra of the pure (unmodified) zeolite demonstrates the presence of the main structural elements, oxygen, silicon, and aluminum (Fig. 2(a–d)).

This ensured that the raw materials were free of impurities. The EDS spectra quantitatively detected the presence of copper particles in the porous medium of the modified zeolites Existing literature suggests that the wet impregnation method guarantees extensive deposition and exchange of materials in the porous medium [40]. The Cu content of each sample is presented in Table 1.

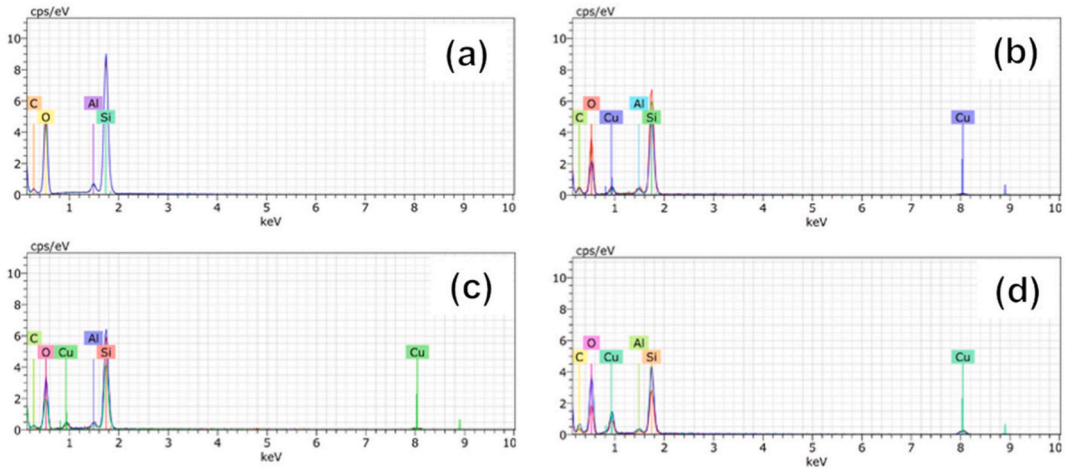

Fig. 2. EDS spectra of zeolite samples before and after copper modification (a) Z40 (unmodified) (b) Z40Cu2, (c) Z40Cu4, (d) Z40Cu8.

Table 1
Composition of the samples modified by metal exchange.

Sample	Element (% weight)				
	Carbon	Oxygen	Aluminium	Silicon	Copper
Z40	40.76	39.12	1.16	18.96	–
Z40Cu2	42.86	34.36	1.14	17.58	4.07
Z40Cu4	32.52	37.05	1.28	21.65	7.5
Z40Cu8	39.55	34.04	0.76	13.24	12.65

3.1.2. X-ray diffraction

Fig. 3 shows the XRD patterns of the copper and capsaicin additives supported on zeolites. By comparison with the XRD pattern of pure CuO, the diffraction peaks at $2\theta = 35.5^{\circ}$ and 38.7° in the XRD pattern of Cu/ZSM-5 were assigned to $(1\ \bar{1}\ 1)$ and (111) reflections of the CuO phase, respectively, confirming that CuO was present in the ZSM-5. The peaks observed in the region between 10° and 30° in the spectrum of Cu/ZSM-5 were essentially identical to those in the spectrum of pure ZSM-5, confirming that the support retained its primary structure after the loading process. Similarly, the XRD patterns of the samples (Fig. 3) show well crystallized materials corresponding to the MFI structure of the ZMS-5 zeolite and the monoclinic crystalline structure of CuO (JCPDS No.85-1326).

3.1.3. Surface area determination by nitrogen adsorption

The nitrogen adsorption assays of the samples modified with metal exchange and capsaicin were obtained at 77 K (Fig. 4(a and b)). All samples exhibit Type I isotherm, according to the IUPAC classification [41]. This behavior was attributed to the microporous structure of the support and the formation of a monolayer of adsorbed gas on its surface [42] which is consistent with the regular nanopore structure of ZSM-5 type zeolites.

The specific surface area of the zeolite decreased with the incorporation of Cu particles, as determined by BET analysis (Fig. 4 (a) and Table 2); these results are in good agreement with those of earlier studies [27]. The BET specific surface area of the capsaicin-modified Z40CPS1 and Z40CPS1,5 samples showed a greater reduction than that of the samples with incorporated copper (Fig. 4 (b) and Table 2). This result was attributed to the molecular size of capsaicin. (1.759 nm), which is larger than that of the copper particles. The mesopore diameter obtained through the BJH method showed that the pore distribution was not affected by the modifications, with pore sizes ranging 3–4 nm in all samples, which evidences the microporous and mesoporous structure of the zeolites. Similarly, the pore volume determined using the HK method exhibited a decreasing trend at higher concentrations of incorporated copper; however, the samples that incorporated capsaicin showed a greater reduction in pore volume (Table 2). The latter was attributed to the fact that biocidal materials are not only supported on the external surface but also enter the pores and cavities of the zeolite.

These results suggest that the reduction in the surface area of the zeolite support materials is due to the blockage of a part of the zeolite pore network by the incorporated materials. In this zeolite, as reported in Table 2, most of the surface area corresponds to pores with diameters below 2 nm. Such results agree with those reported in the literature concerning MFI framework types, such as zeolites ZSM-5 [43]. However, BJH analysis depicts that there are pores between 2 and 20 nm, with a pore size rounding 3.3 nm. The mesopore size distribution can be observed in Fig. S2. Results obtained here suggest that, even when the mesopores are not the main surface area, the low concentrations make it suitable for the incorporation of capsaicin over the zeolite surface. Specifically, BJH analysis shows that the Z40 sample possesses around 15 m^2/g of pores with diameters from 2 to 20 nm. Once copper and capsaicin are supported in the

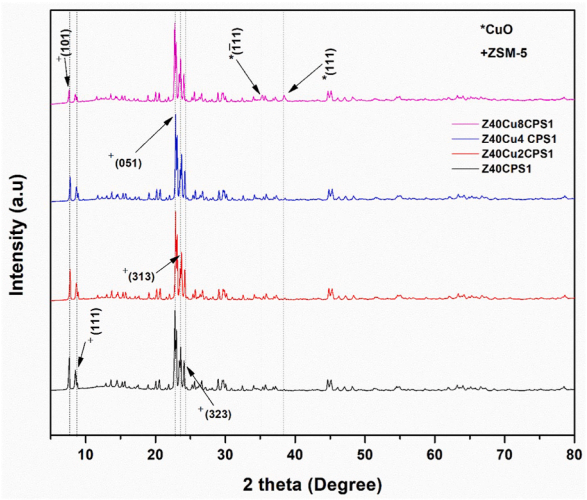

Fig. 3. X-Ray diffraction patterns of the modified zeolites.

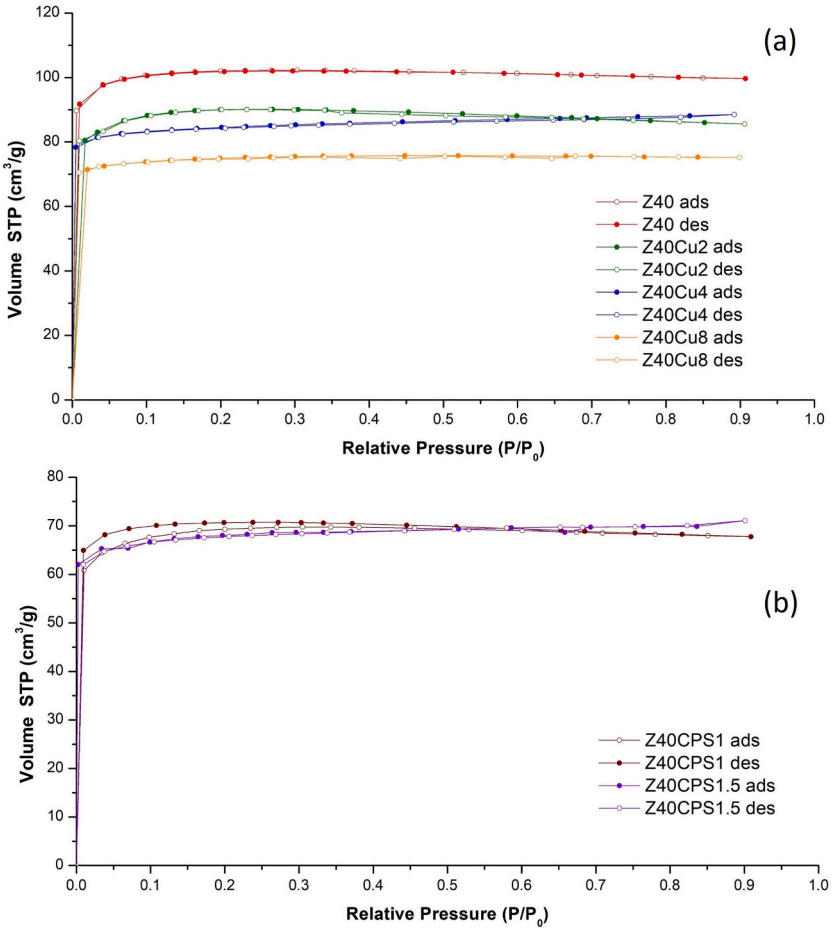

Fig. 4. Nitrogen adsorption isotherms at 77K of (a) metal-modified samples, (b) organic-modified samples.

Table 2
Surface properties of natural and modified zeolites.

Sample	Specific Surface Area[a] (m^2/g)	Mesopores Surface Area[b] (m^2/g)	Mesopore diameter[b] (nm)	Pore volume[c] (cm^3/g)
Z40	303	15	3.3	0.2
Z40Cu2	266	5	3.3	0.1
Z40Cu4	254	3	3.3	0.1
Z40Cu8	223	1	3.8	0.1
Z40CPS1	206	1	3.3	0.10
Z40CPS1,5	197	0	–	–
Z40Cu4CPS1	172	0	–	–

[a] Determined by BET method.
[b] Determined by BJH method.
[c] Determined by HK method.

zeolite, those pores are not open for nitrogen diffusion in the adsorption test. Such results suggest that capsaicin molecules are encapsulated within the zeolite pores. The interaction of the incorporated materials with the encrusting organisms could result in diffusional limitations on the part of the materials supported on the surface, mainly after the incorporation of the organic material.

3.1.4. Fourier transformed infrared spectroscopy

The FTIR spectrum of the ZSM-5 zeolite shows the expected characteristic fingerprint in the range of 1600–500 cm^{-1} (Fig. 5 (a)) [38,39,42]. The bands located between 2500 and 2000 cm^{-1} were attributed to the presence of environmental CO_2 [41]. The spectrum of natural capsaicin (95% purity) shows in which the 3306 cm^{-1} bands corresponding to aminoacidic bonds (N–H) at 3306 cm^{-1}, aliphatic stretching vibrations (C–H) in the range of 2925 to 2858 cm^{-1}, and carbonyl stretching vibrations at 1627 cm^{-1}. Additionally, stretching vibrations (C–C) were detected in the range of 1551–1514 cm^{-1} and an out of plane bending C–H vibrations was

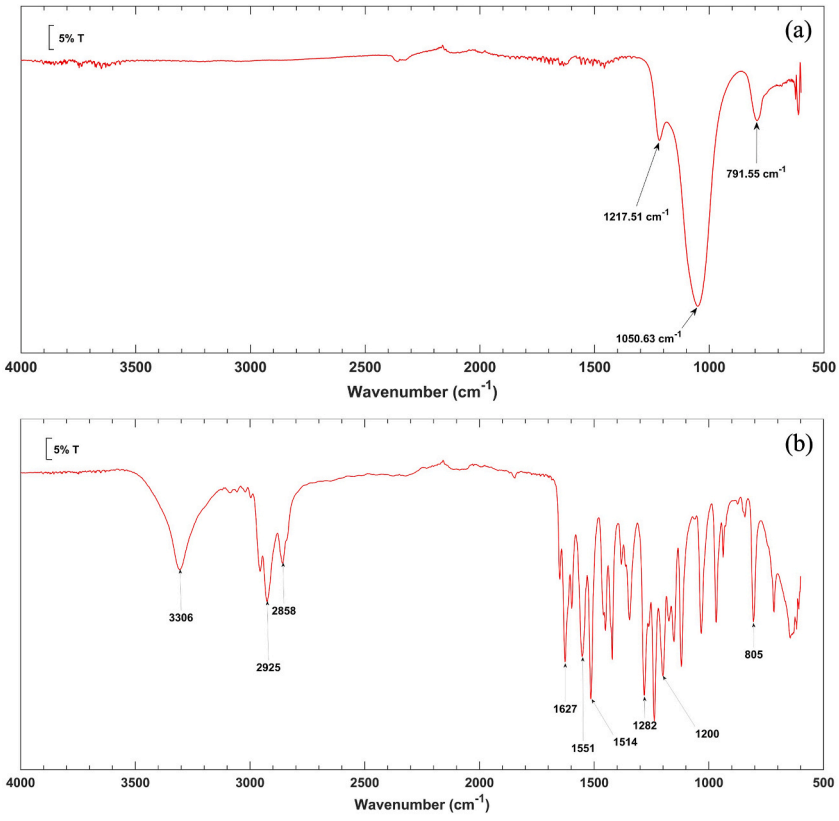

Fig. 5. FTIR spectra of (a) ZSM-5 synthetic zeolite and (b) natural capsaicin (95% purity).

observed between 870 and 805 cm^{-1}, which was attributed to the vibration of the aromatic ring (Fig. 5 (b)).

In the spectra of the metal modified zeolite samples Z40Cu2, Z40Cu4, and Z40Cu8 (Fig. 6 (a)), the band at 1217.51 cm^{-1} is redshifted by 2.4 cm^{-1}, 5.5 cm^{-1}, 6.1 cm^{-1}, respectively, relative to that in the IR spectrum of the support material. Similarly, the band located at 1050.63 cm^{-1} in the spectrum of Z40 is shifted to lower wavenumbers as the copper concentration increases. Similar studies by Razavi and Loghman Estarki suggested that such changes are attributable to the distortion in the zeolite crystal lattice caused by the nanoparticles and the interaction between the nanoparticles and the zeolite matrix produced by electrostatic forces arising from the negative charges of the support matrix [32].

The FTIR spectra of the capsaicin-modified zeolite samples confirmed the presence of organic molecules in the support matrix by the appearance of a new peak in the region between 876 and 874 cm^{-1} (Fig. 6 (b)). This band is associated with the out of plane C–H bending vibrations of the aromatic group of the capsaicin molecule [44–46]. Furthermore, the wavenumber of this peak varies according to the concentration of capsaicin, being centered at 876.35 cm^{-1}, 875.73 cm^{-1} and 874.82 cm^{-1} in the spectra of Z40CPS1, Z40CPS1,5 and Z40CPS5 respectively. This trend was confirmed using a zeolite sample modified with 5% capsaicin (Z40CPS5). The absence of other vibrational modes of capsaicin may be explained by its interaction with the zeolite, suggesting that it is adsorbed on the surface of the support. The spectra of the samples modified with copper and capsaicin verify that organic molecules can be incorporated into the support medium, even in the presence of copper nanoparticles (Fig. 7) owing to the large surface area of the copper-modified zeolite samples, in which the surface of the support is unsaturated, thereby allowing the subsequent deposition of capsaicin.

3.2. Computational measurement of capsaicin molecular size

Previous studies concerning the use of capsaicin refer to its chemical properties but not its molecular size; however, this information is of great importance because the size of a molecules determines whether it diffuses within the pores and channels of the zeolite or whether it is only deposited over the outer surface and therefore affects the physicochemical modification of the zeolite. The Avogadro Software 1.2.0 was used to approximate the molecular size of capsaicin. The molecular geometry of the capsaicin molecule (IUPAC name: 8-methyl-N-vanillyl-6-nonenamide) was optimized according to low-energy conformation criteria by searching for a global minimum energy using the Merck molecular force field method (MMFF94). Using the obtained geometry, the maximum stable length of the capsaicin molecule was determined by considering the size of each atom (H, C, O, and N) and the length of the bonds, which can be single or double [47]. This computational analysis established the molecular size of capsaicin, demonstrating that the

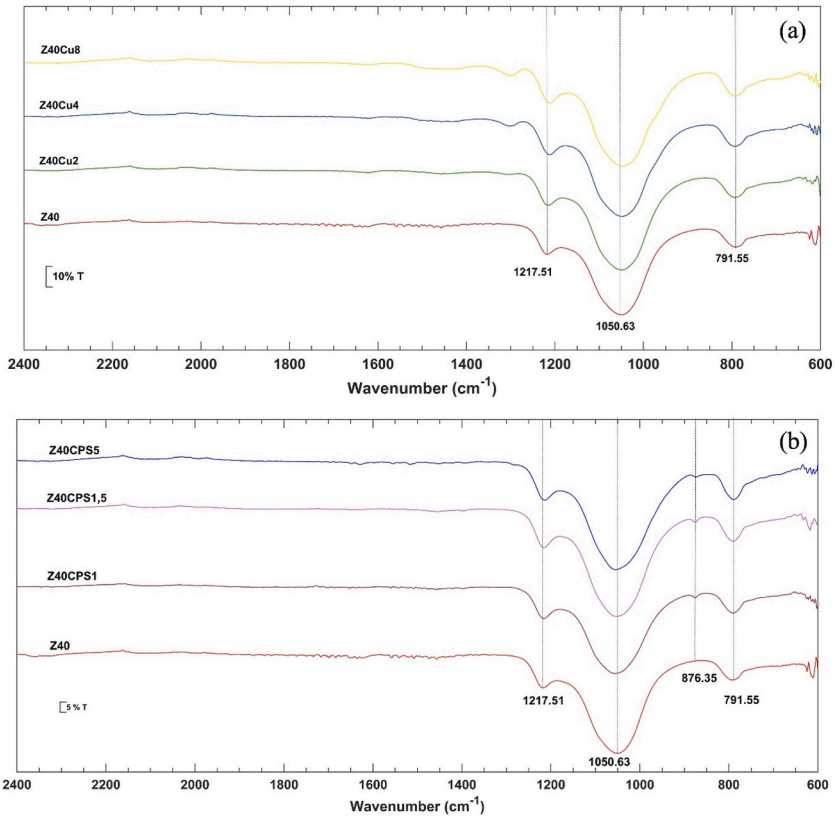

Fig. 6. FTIR spectra of (a) ZSM-5 and copper-modified zeolites and (b) capsaicin-modified ZSM-5 zeolite samples.

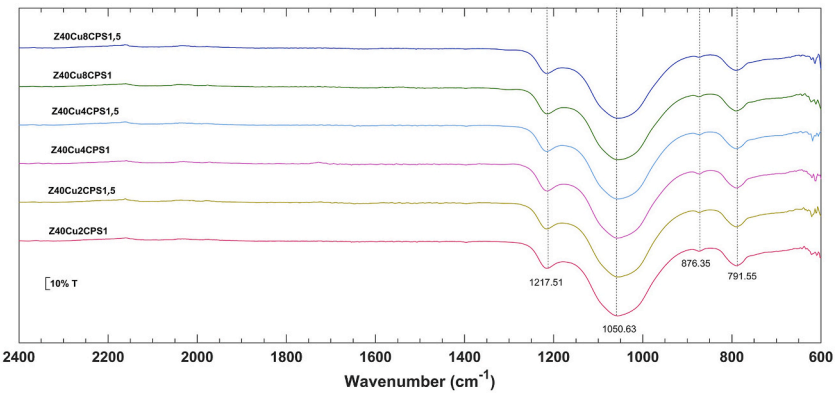

Fig. 7. FTIR spectra of ZSM-5 zeolite after metal and organic modifications.

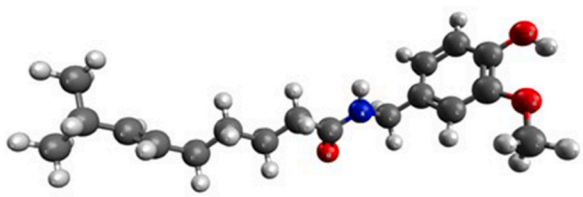

Fig. 8. Molecular structure of capsaicin.

incorporation of capsaicin into the porous structure of the zeolite is feasible and thereby indicating the suitability of this microporous material as a support. The structure of capsaicin is shown in Fig. 8. This conformation is stable, with an energy of −8.14131 kJ/mol, which indicated the feasibility of this structure. According to this analysis, capsaicin has a maximum possible length of 17,590 Å (1.759 nm), approximately half the size of the mean mesopore diameter of the parent zeolite (3 nm). Kambaine et al. [48] determined by Molecular Dynamics Simulation that the gyration radius of the capsaicin molecule in different solvents rounds from 0.4 to 0.45 nm; such information coincides with data reported by Graham et al. [49]. The radius of gyration can be considered an indirect measure of conformation, and the molecule's interaction with systems such as proteins or membranes. Additionally, due to their geometric configuration, the higher distance among the carbon atoms in the cross-section of the aromatic group of the capsaicin molecule rounds 0.48 nm [50].

It's worth noting that, in addition to capsaicin, other organic molecules with similar structures have also been successfully incorporated into zeolitic materials. For instance, Rabiee & Rabiee [51] deposited capsaicin onto ZSM-5 zeolite to achieve controlled delivery of capsaicin as a theranostic agent. Afterwards, Musielak et al. [52] supported curcumin molecules in commercial Faujasites, and recently, Q. Tan et al. [53], reported the encapsulation of indole, a heterocyclic molecule, in Beta zeolites as an antibacterial material with controllable release property. Thus, it is reasonable to assume that capsaicin can be incorporated within the crystalline structure of the zeolite, lodging inside the pores and cavities.

3.3. *Antifouling assays: the role of the biocide and microporous support in the abatement of marine bacteria*

Of the 13 samples analyzed, 10 (76.9%) were active against the marine bacterial strains of *I. loihiensis* UCO25, *Pseudoalteromonas* sp. UCO92 and *H. boliviensis* UCO24; the three remaining samples (23.0 %) did not inhibit bacterial growth (Table 3 and Table 4). To evaluate the effect of the copper and capsaicin concentrations, the samples were compared via grouping and classification studies. Fisher's test of the least significant difference (LSD) was applied with a reliability level of 95% (Supplementary material, Table S1). The contribution of the support material to the inhibition of bacterial growth was initially studied without a visible halo. This analysis suggested that the zeolite primarily served as a support for the biocidal compounds. Notably, the copper contents in the samples modified with the metallic inhibitor had a significantly impact on the inhibition capacity of the material with a 95% confidence level. An increase in the copper concentration resulted in a larger, implying a stronger biocidal effect. The bactericide effect of Cu ions could be attributed by the adherence to bacterial cytomembrane and cytoderm via electron interaction damaging the intracellular protein of bacteria. Copper exposure seems to induce drastic changes in the lipid composition of the bacterial cell membrane and to modulate the abundance of proteins functionally known to be involved in copper cell homeostasis [54].

Fig. 9 displays the changes in inhibition halos for *I. loihiensis* UCO25 (Fig. 9 (a)), *Pseudoalteromonas* sp. UCO92 (Fig. 9 (b)) and *H. boliviensis* UCO24 (Fig. 9 (c)) as a function of capsaicin and copper loading. In samples formulated with both capsaicin and copper, an increase in the halo diameter was observed as the copper concentration increased, irrespective of the capsaicin content. Conversely, zeolites formulated with capsaicin alone exhibited a reduction in the halo diameter. It is worth noting that neither pure capsaicin nor capsaicin-modified samples presented inhibition halos. This phenomenon was attributed to the hydrophobic nature of capsaicin [55]. In this sense, it could be assumed that the samples become more hydrophobic, mainly after adding the capsaicin molecules. Additionally, the substitution of the strong Brønsted sites present in the NH_4^+ compensating cations for weak Cu^{2+} Lewis acid sites could reduce the water adsorption capacities, as those acidic centers are the main water interacting active sites [27,56].

In addition, among the samples modified with both biocidal materials, Z40Cu8CPS1 formed the largest inhibition halo, followed by Z40Cu8CPS1,5. In this study, pure copper nitrate was not investigated as an inhibitory material, as its biocidal effect has been demonstrated in other investigations [57], However, the use of pure copper in high concentrations could be harmful to aquatic ecosystems, and its inhibitory effect may be short-lived due to its fast diffusion. As a water-soluble salt, copper nitrate dissociates into ions and readily diffuses in aquatic media [58].

Fisher's analysis of these samples showed that subsequent modification of the material with 8% p/p copper with 1% p/p and 1.5% p/p did not result in a significant difference. In addition, significant differences were obtained from the assays using 2%, 4%, and 8% w/w copper-modified samples showed significant differences regardless of the incorporated capsaicin content, at a 95% confidence interval (Supplementary material, Table S1).

Table 3
Bacterial inhibition halos to *Idiomarina loihiensis*., *Pseudoalteromonas* spp. and *Halomonas boliviensis* using parent and modified zeolites.

Bacterial strain	Inhibition zone (mm)							Inhibition zone Positive Control			
	Z40	**Z40Cu2**	**Z40Cu4**	**Z40Cu8**	**CPS**	**Z40CPS1**	**Z40CPS1,5**	**FOS200**	**TE30**	**FOX30**	**LEV5**
UCO25	42.0 ± 2.0	42.3 ± 2.1	49.7 ± 0.6	56.0 ± 1.0	0.0 ± 0.0	0.0 ± 0.0	0.0 ± 0.0	18.7 ± 1.5	0.0 ± 0.0	24.3 ± 2.5	23.0 ± 2.6
UCO92	32.0 ± 2.0	43.3 ± 0.6	47.3 ± 1.2	50.7 ± 1.2	0.0 ± 0.0	0.0 ± 0.0	0.0 ± 0.0	0.0 ± 0.0	0.0 ± 0.0	19.3 ± 1.5	26.3 ± 0.6
UCO24	36.7 ± 3.1	47.0 ± 1.0	57.0 ± 1.0	61.0 ± 1.0	0.0 ± 0.0	0.0 ± 0.0	0.0 ± 0.0	0.0 ± 0.0	0.0 ± 0.0	16.7 ± 2.1	21.3 ± 0.6

Abbreviations: UCO25*; Idiomarina loihiensis*, UCO92; *Pseudoalteromonas* spp, UCO24 *Halomonas boliviensis** Mean values with significant differences ($P < 0.05$) in Table S1 (Supplementary Materials).

Table 4
Continuation Table 3 bacterial inhibition halos to *Idiomarina loihiensis*., *Pseudoalteromonas* spp. and *Halomonas boliviensis* using parent and modified zeolites.

Bacterial strain	Inhibition zone (mm)							Inhibition zone Positive Control		
	Z40Cu2CPS1	**Z40Cu4CPS1**	**Z40Cu8CPS1**	**Z40Cu2CPS1,5**	**Z40Cu4CPS1,5**	**Z40Cu8CPS1,5**	**FOS200**	**TE30**	**FOX30**	**LEV5**
UCO25	42.0 ± 2.0	42.3 ± 2.1	49.7 ± 0.6	56.0 ± 1.0	0.0 ± 0.0	0.0 ± 0.0	18.7 ± 1.5	0.0 ± 0.0	24.3 ± 2.5	23.0 ± 2.6
UCO92	33.7 ± 2.3	45.7 ± 1.2	51.0 ± 1.7	32.7 ± 2.3	41.7 ± 1.5	48.0 ± 2.6	0.0 ± 0.0	0.0 ± 0.0	19.3 ± 1.5	26.3 ± 0.6
UCO24	30.7 ± 1.2	45.3 ± 1.2	52.7 ± 3.1	32.7 ± 2.3	43.3 ± 0.6	46.7 ± 0.6	0.0 ± 0.0	0.0 ± 0.0	16.7 ± 2.1	21.3 ± 0.6

Abbreviations: UCO25*; Idiomarina loihiensis*, UCO92; *Pseudoalteromonas* spp, UCO24 *Halomonas boliviensis** Mean values with significant differences ($P < 0.05$) in Table S1 (Supplementary Materials).

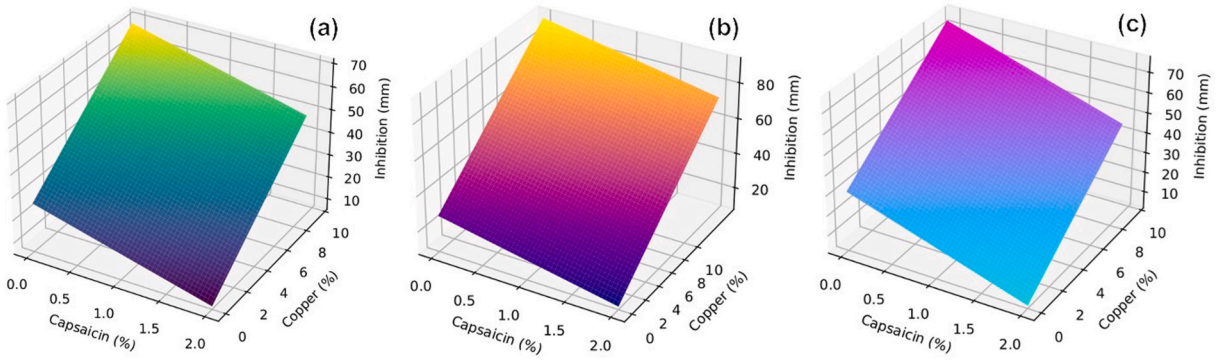

Fig. 9. Inhibition halos as a function of copper and capsaicin contents: (a) *Idiomarina loihiensis* UCO25 (b) *Pseudoalteromonas* sp. UCO92 (c) *Halomonas boliviensis* UCO24.

Capsaicin can also block contact between copper cations and aqueous media. This is in good agreement with the results obtained from the surface characterization, in which a reduction in the surface area of the samples containing capsaicin was observed. Capsaicin molecules were incorporated in the pores of the zeolite and therefore blocked the diffusion of other molecules and affected the contact between the bacteria and copper sites. However, even when capsaicin did not result in significantly different inhibition, through comparative analysis revealed that samples Z40Cu8, Z40Cu8CPS1, and Z40Cu8CPS1,5 formed halos with larger diameters and therefore had the strongest biocidal effect. This suggests that, as it has been reported [59], capsaicin decreases the growth rate of bacteria strains and some other microorganisms [60]; however, its dispersion in the medium is limited. The interaction mechanism of capsaicin to inhibit the bacteria growth could be attributed partially to its protein inhibiting qualities and the improvement of the surface hydrophobic properties [60]. Similar studies conducted using other bacteria species, specifically *Pseudomona Aeruginosa*, has depicted that even when capsaicin doesn't migrate to water media, it can be released from the support surface to kill bacteria when the pH of the local environment decreases, which is triggered by the reproduction of bacteria in the environment [22]. Similarly, Guo et al. showed a lack of direct action of capsaicin against some bacterial strains, however a potent synergistic action in the case of combinatory use of these substances in a dose-dependent manner was also shown [61].

Results obtained here suggest that copper and capsaicin act as the primary and reinforcement biocides, respectively, and that zeolite acts as a support, controlling the delivery of the biocides. The copper particles, located in the ZSM-5 pores with a pore configuration that favors controlled delivery, could diffuse and interact with the surrounding microorganisms, acting as the primary biocide. On the other hand, the capsaicin molecules, encapsulated mainly in the mesopores, diffuse slowly in the presence of water due to their hydrophobic nature but can act as a reinforcement biocide to extend their useful life. Nevertheless, further studies must be conducted to depict the specific effects of both biocidal agents and to unveil the way to control their release into water media, including controlled delivery assays, to use the studied materials for real applications. Additionally, studies using different types of zeolites with varying porosities, such as Y zeolites, or using mesoporous zeolites such as MCM-41, must be conducted to study the influence of the presence of larger pores, such as the super cages of Y-zeolite, on the biocides' support and release.

4. Conclusions

Zeolites modified with copper nanoparticles and capsaicin molecules are effective as biocidal agents. Copper nanoparticles inhibit the growth of bacteria while capsaicin acts as a reinforcing biocide. Similarly, the microporous structure of the zeolite increases the contact surface area and retention of biocidal agents, thus enhancing their interaction with microorganisms. Modification with copper nanoparticles and capsaicin molecules affects the surface physicochemical characteristics of synthetic zeolites. The incorporation of copper nanoparticles reduces both the surface area of the zeolite and the volume of the micropores and mesopores of the support. However, incorporating the large, hydrophobic capsaicin molecule, mainly on the larger pores of the zeolite, affects the surface area and pore volume of the support to a greater extent, limiting the diffusion of water into the pores and limiting the interaction between the bacteria and active compounds. The presence of higher concentrations of capsaicin could limit the access and interaction of some of the metallic particles with microorganisms.

Funding

The research was funded by National Agency for Research and Development (ANID, by its acronym in Spanish), under the Ministry of Science, Government of Chile. FONDECYT INICIACION Project 11190358 and FONDECYT REGULAR project 1231376.

Ethical approval

This article does not contain any studies with human or animal subjects performed by any of the authors.

Data availability statement

The authors confirm that the data supporting the findings of this study are available within the article. In addition, the datasets used and/or analyzed during the current study are available from the corresponding author on reasonable request.

CRediT authorship contribution statement

I. Huenuvil-Pacheco: Methodology, Formal analysis. **A.F. Jaramillo:** Writing – original draft, Supervision, Resources, Project administration, Investigation, Formal analysis. **N.J. Abreu:** Writing – original draft, Methodology, Investigation. **K. Garrido-Miranda:** Formal analysis. **G. Sánchez-Sanhueza:** Methodology, Formal analysis. **G. González-Rocha:** Formal analysis. **C. Medina:** Writing – review & editing. **L.F. Montoya:** Writing – review & editing. **J.P. Sanhueza:** Writing – original draft. **M.F. Melendrez:** Writing – original draft, Resources, Investigation.

Declaration of competing interest

The authors declare the following financial interests/personal relationships which may be considered as potential competing interests: Andres Jaramillo reports financial support was provided by University of the Frontier.

Acknowledgments

AFJ extends thanks to ANID for the support received through the FONDECYT INICIACION Project 11190358 and FONDECYT REGULAR project 1231376. NJA extends thanks to ANID for the support received through the FONDECYT POSTDOCTORADO project 3210158. MFM acknowledges ANID for their support through the following projects: FONDEQUIP Project N°EQM150139, EQM190002, PIA/APOYO CCTE AFB170007. MFM also expresses gratitude to Valentina Lamilla and Juliana Meléndrez for their enormous support.

Appendix A. Supplementary data

Supplementary data to this article can be found online at https://doi.org/10.1016/j.heliyon.2024.e27182.

References

[1] D.M. Yebra, S. Kiil, K. Dam-Johansen, Antifouling technology—past, present and future steps towards efficient and environmentally friendly antifouling coatings, Prog. Org. Coating 50 (2004) 75–104, https://doi.org/10.1016/j.porgcoat.2003.06.001.
[2] M. Camps, J. Briand, L. Guentas-Dombrowsky, G. Culioli, A. Bazire, Y. Blache, Antifouling activity of commercial biocides vs. natural and natural-derived products assessed by marine bacteria adhesion bioassay, Mar. Pollut. Bull. 62 (2011) 1032–1040, https://doi.org/10.1016/j.marpolbul.2011.02.031.
[3] I. Amara, W. Miled, R. Ben Slama, N. Ladhari, Antifouling processes and toxicity effects of antifouling paints on marine environment. A review, Environ. Toxicol. Pharmacol. 57 (2018) 115–130, https://doi.org/10.1016/j.etap.2017.12.001.
[4] Z. He, X. Lan, Q. Hu, H. Li, L. Li, J. Mao, Antifouling strategies based on super-phobic polymer materials, Prog. Org. Coating 157 (2021) 106285, https://doi.org/10.1016/j.porgcoat.2021.106285.
[5] J.R. Almeida, V. Vasconcelos, Natural antifouling compounds: effectiveness in preventing invertebrate settlement and adhesion, Biotechnol. Adv. 33 (2015) 343–357, https://doi.org/10.1016/j.biotechadv.2015.01.013.
[6] V. Ferreira, M.D. Pavlaki, R. Martins, M.S. Monteiro, F. Maia, J. Tedim, A.M.V.M. Soares, R. Calado, S. Loureiro, Effects of nanostructure antifouling biocides towards a coral species in the context of global changes, Sci. Total Environ. 799 (2021) 149324, https://doi.org/10.1016/j.scitotenv.2021.149324.
[7] F. Nobakht-Kolur, M. Zeinoddini, M.M.A. Harandi, F.A. Abi, P. Jadidi, Effects of soft marine fouling on wave-induced forces in floating aquaculture cages: physical model testing under regular waves, Ocean Eng 238 (2021) 109759, https://doi.org/10.1016/j.oceaneng.2021.109759.
[8] P. Berillis, E. Mente, K.A. Kormas, The use of copper alloy in aquaculture fish net pens: mechanical, economic and environmental advantages, J. Fish. 11 (2017) 1–3, https://doi.org/10.21767/1307-234X.1000134.
[9] M.A. Champ, A review of organotin regulatory strategies, pending actions, related costs and benefits, Sci. Total Environ. 258 (2000) 21–71, https://doi.org/10.1016/S0048-9697(00)00506-4.
[10] S. Palanichamy, G. Subramanian, Antifouling properties of marine bacteriocin incorporated epoxy based paint, Prog. Org. Coating 103 (2017) 33–39, https://doi.org/10.1016/j.porgcoat.2016.11.020.
[11] M. Lagerström, E. Ytreberg, Quantification of Cu and Zn in antifouling paint films by XRF, Talanta 223 (2021) 121820, https://doi.org/10.1016/j.talanta.2020.121820.
[12] J.G. Rodríguez, I. Tueros, Á. Borja, J. Franco, J. Ignacio García Alonso, J.M. Garmendia, I. Muxika, C. Sariego, V. Valencia, Butyltin compounds, sterility and imposex assessment in Nassarius reticulatus (Linnaeus, 1758), prior to the 2008 European ban on TBT antifouling paints, within Basque ports and along coastal areas, Continent. Shelf Res. 29 (2009) 1165–1173, https://doi.org/10.1016/j.csr.2009.01.005.
[13] A.R. Neves, J.R. Almeida, F. Carvalhal, A. Câmara, S. Pereira, J. Antunes, V. Vasconcelos, M. Pinto, E.R. Silva, E. Sousa, M. Correia-da-Silva, Overcoming environmental problems of biocides: synthetic bile acid derivatives as a sustainable alternative, Ecotoxicol. Environ. Saf. 187 (2020) 109812, https://doi.org/10.1016/j.ecoenv.2019.109812.
[14] X. Zhai, P. Ju, F. Guan, Y. Ren, X. Liu, N. Wang, Y. Zhang, J. Duan, C. Wang, B. Hou, Electrodeposition of capsaicin-induced ZnO/Zn nanopillar films for marine antifouling and antimicrobial corrosion, Surf. Coating. Technol. 397 (2020) 125959, https://doi.org/10.1016/j.surfcoat.2020.125959.
[15] I. Omae, General aspects of tin-free antifouling paints, Chem. Rev. 103 (2003) 3431–3448, https://doi.org/10.1021/cr030669z.
[16] X. Lin, X. Huang, C. Zeng, W. Wang, C. Ding, J. Xu, Q. He, B. Guo, Poly(vinyl alcohol) hydrogels integrated with cuprous oxide–tannic acid submicroparticles for enhanced mechanical properties and synergetic antibiofouling, J. Colloid Interface Sci. 535 (2019) 491–498, https://doi.org/10.1016/j.jcis.2018.10.017.
[17] N. Bellotti, B. Amo, R. Romagnoli, Caesalpinia spinosa tannin derivatives for antifouling formulations, Procedia Mater. Sci. 1 (2012) 259–265, https://doi.org/10.1016/j.mspro.2012.06.035.

[18] H. Palza, K. Delgado, N. Moraga, S.-H. Wang Molina, Polypropylene in the melt state as a medium for in situ synthesis of copper nanoparticles, AIChE J. 60 (2014) 3406–3411, https://doi.org/10.1002/aic.14549.
[19] Y. Qi, W. Liang, Q. Miao, H. Lin, H. An, Y. Liu, S. Zuo, H. Ma, Corrosion behavior and antifouling ability of Cu-Zn-Al/Zn-Al composite coating on Q235 steel, Surf. Coating. Technol. 405 (2021) 126614, https://doi.org/10.1016/j.surfcoat.2020.126614.
[20] Z. Jia, Y. Liu, Y. Wang, Y. Gong, P. Jin, X. Suo, H. Li, Flame spray fabrication of polyethylene-Cu composite coatings with enwrapped structures: a new route for constructing antifouling layers, Surf. Coating. Technol. 309 (2017) 872–879, https://doi.org/10.1016/j.surfcoat.2016.10.071.
[21] X. Hao, W. Wang, Z. Yang, L. Yue, H. Sun, H. Wang, Z. Guo, F. Cheng, S. Chen, pH responsive antifouling and antibacterial multilayer films with Self-healing performance, Chem. Eng. J. 356 (2019) 130–141, https://doi.org/10.1016/j.cej.2018.08.181.
[22] X. Hao, S. Chen, D. Qin, M. Zhang, W. Li, J. Fan, C. Wang, M. Dong, J. Zhang, F. Cheng, Z. Guo, Antifouling and antibacterial behaviors of capsaicin-based pH responsive smart coatings in marine environments, Mater. Sci. Eng. C. 108 (2020) 110361, https://doi.org/10.1016/j.msec.2019.110361.
[23] P. Lalueza, M. Monzón, M. Arruebo, J. Santamaría, Bactericidal effects of different silver-containing materials, Mater. Res. Bull. 46 (2011) 2070–2076, https://doi.org/10.1016/j.materresbull.2011.06.041.
[24] J.L. Cerrillo, A.E. Palomares, F. Rey, Silver exchanged zeolites as bactericidal additives in polymeric materials, Microporous Mesoporous Mater. 305 (2020) 110367, https://doi.org/10.1016/j.micromeso.2020.110367.
[25] P. Baile, L. Vidal, A. Canals, A modified zeolite/iron oxide composite as a sorbent for magnetic dispersive solid-phase extraction for the preconcentration of nonsteroidal anti-inflammatory drugs in water and urine samples, J. Chromatogr. A. 1603 (2019) 33–43, https://doi.org/10.1016/j.chroma.2019.06.039.
[26] S. Park, N. Jiang, Morphological synthesis of zeolites, in: Zeolites Catal., Wiley, 2010, pp. 131–153, https://doi.org/10.1002/9783527630295.ch5.
[27] N.J. Abreu, H. Valdés, C.A. Zaror, F. Azzolina-Jury, M.F. Meléndrez, Ethylene adsorption onto natural and transition metal modified Chilean zeolite: an operando DRIFTS approach, Microporous Mesoporous Mater. 274 (2019) 138–148, https://doi.org/10.1016/j.micromeso.2018.07.043.
[28] Z. Zijun, G. Effeney, G.J. Millar, M. Stephen, Synthesis and cation exchange capacity of zeolite W from ultra-fine natural zeolite waste, Environ. Technol. Innov. 23 (2021) 101595, https://doi.org/10.1016/j.eti.2021.101595.
[29] G.J. Millar, S.J. Couperthwaite, K. Alyuz, Behaviour of natural zeolites used for the treatment of simulated and actual coal seam gas water, J. Environ. Chem. Eng. 4 (2016) 1918–1928, https://doi.org/10.1016/j.jece.2016.03.014.
[30] C. Karavasili, E.P. Amanatiadou, E. Kontogiannidou, G.K. Eleftheriadis, N. Bouropoulos, E. Pavlidou, I. Kontopoulou, I.S. Vizirianakis, D.G. Fatouros, Comparison of different zeolite framework types as carriers for the oral delivery of the poorly soluble drug indomethacin, Int. J. Pharm. 528 (2017) 76–87, https://doi.org/10.1016/j.ijpharm.2017.05.061.
[31] G. Cik, H. Bujdakov, F. Sersen, Study of fungicidal and antibacterial effect of the Cu (II) -complexes of thiophene oligomers synthesized in ZSM-5 zeolite channels, Chemosphere 44 (2001) 313–319, https://doi.org/10.1016/s0045-6535(00)00306-4.
[32] H. Zhang, I. bin Samsudin, S. Jaenicke, G.-K. Chuah, Zeolites in catalysis: sustainable synthesis and its impact on properties and applications, Catal. Sci. Technol. 12 (2022) 6024–6039, https://doi.org/10.1039/D2CY01325H.
[33] A.A. Alswat, M. Bin Ahmad, T.A. Saleh, Zeolite modified with copper oxide and iron oxide for lead and arsenic adsorption from aqueous solutions, J. Water Supply Res. Technol. 65 (2016) 465–479, https://doi.org/10.2166/aqua.2016.014.
[34] R. Shoja Razavi, M.R. Loghman-Estarki, Synthesis and characterizations of copper oxide nanoparticles within zeolite Y, J. Clust. Sci. 23 (2012) 1097–1106, https://doi.org/10.1007/s10876-012-0502-y.
[35] J.-A. Kim, M. Kong, J.-H. Kim, K.-S. Chung, C.-Y. Eom, H.-O. Yoon, Identification of marine bacteria affecting lithium adsorbents in seawater, Environ. Geochem. Health 35 (2013) 311–315, https://doi.org/10.1007/s10653-012-9495-6.
[36] Y. Leng, R. Colston, A. Soares, Understanding the biochemical characteristics of struvite bio-mineralising microorganisms and their future in nutrient recovery, Chemosphere 247 (2020) 125799, https://doi.org/10.1016/j.chemosphere.2019.125799.
[37] S. Wu, G. Liu, W. Jin, P. Xiu, C. Sun, Antibiofilm and anti-infection of a marine bacterial exopolysaccharide against Pseudomonas aeruginosa, Front. Microbiol. 7 (2016), https://doi.org/10.3389/fmicb.2016.00102.
[38] G. Wu, X. Wang, Y. Yang, L. Li, G. Wang, N. Guan, Confirmation of NH species in the framework of nitrogen-incorporated ZSM-5 zeolite by experimental and theoretical studies, Microporous Mesoporous Mater. 127 (2010) 25–31, https://doi.org/10.1016/j.micromeso.2009.06.025.
[39] C. Liu, W. Gu, D. Kong, H. Guo, The significant effects of the alkali-metal cations on ZSM-5 zeolite synthesis: from mechanism to morphology, Microporous Mesoporous Mater. 183 (2014) 30–36, https://doi.org/10.1016/j.micromeso.2013.08.037.
[40] B.A.T. Mehrabadi, S. Eskandari, U. Khan, R.D. White, J.R. Regalbuto, A review of preparation methods for supported metal catalysts, Adv. Catal. (2017) 1–35, https://doi.org/10.1016/bs.acat.2017.10.001.
[41] M. Thommes, K. Kaneko, A.V. Neimark, J.P. Olivier, F. Rodriguez-Reinoso, J. Rouquerol, K.S.W. Sing, Physisorption of gases, with special reference to the evaluation of surface area and pore size distribution (IUPAC Technical Report), Pure Appl. Chem. 87 (2015) 1051–1069, https://doi.org/10.1515/pac-2014-1117.
[42] C. Boruban, E. Nalbant Esenturk, Synthesis of CuO nanostructures on zeolite-Y and investigation of their CO2 adsorption properties, J. Mater. Res. 32 (2017) 3669–3678, https://doi.org/10.1557/jmr.2017.337.
[43] L. Zoubida, B. Hichem, The nanostructure zeolites MFI-type ZSM5, in: Nanocrystals and Nanostructures, 2018, pp. 43–62, https://doi.org/10.5772/intechopen.77020.
[44] M. Çınar, B. Alım, Z. Alım, E. Şakar, Determination of the molecular structure and spectroscopic properties of capsaicin, Radiat. Phys. Chem. 208 (2023) 110879, https://doi.org/10.1016/j.radphyschem.2023.110879.
[45] A. El Kaaby Ekhlas, N. Al Hattab Zahra, A. Ai-Anny Jenan, FT-IR Identification of Capsaicin from callus and seedling of chilli pepper plants Capsicum annuum L. in vitro, Int. J. Multidiscip. Curr. Res. 4 (2016) 1144–1146.
[46] J. Sherin Percy Prema Leela, R. Hemamalini, S. Muthu, A.A. Al-Saadi, Spectroscopic investigation (FTIR spectrum), NBO, HOMO–LUMO energies, NLO and thermodynamic properties of 8-Methyl-N-vanillyl-6-nonenamideby DFT methods, Spectrochim. Acta Part A Mol. Biomol. Spectrosc. 146 (2015) 177–186, https://doi.org/10.1016/j.saa.2015.03.027.
[47] T. a Halgren, Merck molecular force field. I. Basis, form, scope, parameterization, and performance of MMFF94, J. Comput. Chem. 17 (1996) 490–519, https://doi.org/10.1002/(SICI)1096-987X.
[48] N.D. Kambaine, D.M. Shadrack, S.A.H. Vuai, Conformations and stability of capsaicin in bulk solvents : a molecular dynamics study, J. Mol. Liq. 345 (2022) 117794, https://doi.org/10.1016/j.molliq.2021.117794.
[49] J.A. Graham, J.W. Essex, S. Khalid, PyCGTOOL: automated generation of coarse-grained molecular dynamics models from atomistic trajectories, J. Chem. Inf. Model. 57 (2017) 650–656, https://doi.org/10.1021/acs.jcim.7b00096.
[50] M. Çınar, B. Alım, Z. Alım, S. Erdem, Determination of the molecular structure and spectroscopic properties of capsaicin, Radiat. Phys. Chem. 208 (2023) 110879, https://doi.org/10.1016/j.radphyschem.2023.110879.
[51] N. Rabiee, M. Rabiee, A promising stimuli-responsive nanocomposite as a theranostic agent for targeted delivery, Bioeng. Res. 1 (2019) 27–36, https://doi.org/10.22034/jbr.2019.84394, because.
[52] E. Musielak, A. Feliczak-Guzik, M. Jaroniec, I. Nowak, Modification and functionalization of zeolites for curcumin uptake, Materials 15 (2022) 6316, https://doi.org/10.3390/ma15186316.
[53] Q. Tan, Y. Li, T. Li, Y. Huang, E. Xing, Y. Bi, X. Zhang, Q. Chen, W. Li, Zeolite beta in situ encapsulation of indole and its derivatives as controlled release formulations for antibacterial, Microporous Mesoporous Mater. 325 (2021) 111342, https://doi.org/10.1016/j.micromeso.2021.111342.
[54] L. Favre, A. Ortalo-Magné, L. Kerloch, C. Pichereaux, B. Misson, J.F. Briand, C. Garnier, G. Culioli, Metabolomic and proteomic changes induced by growth inhibitory concentrations of copper in the biofilm-forming marine bacterium: Pseudoalteromonas lipolytica, Metallomics 11 (2019) 1887–1899, https://doi.org/10.1039/c9mt00184k.
[55] X. Tao, L. Zhan, Y. Huang, P. Li, B. Liu, P. Chen, Preparation, characterization and evaluation of capsaicin-loaded indica rice starch nanoparticles, Food Chem. 386 (2022), https://doi.org/10.1016/j.foodchem.2022.132692.

[56] S.E. Russell, J. María, G. Carballo, C. Orellana-tavra, D. Fairen, R.E. Morris, A comparison of copper and acid site zeolites for the production of nitric oxide for biomedical applications, Dalt. Trans. 46 (2017) 3915–3920, https://doi.org/10.1039/C7DT00195A.
[57] X. Santos, J. Rodr, F. Guill, J. Pozuelo, D. Videira-quintela, O. Mart, Capability of copper hydroxy nitrate (Cu2(OH)3NO3) as an additive to develop antibacterial polymer contact surfaces: potential for food packaging applications, Polymers 15 (2023) 1661, https://doi.org/10.3390/polym15071661.
[58] A.F. Jaramillo, S.A. Riquelme, G. Sánchez-Sanhueza, C. Medina, F. Solís-Pomar, D. Rojas, C. Montalba, M.F. Melendrez, E. Pérez-Tijerina, Comparative study of the antimicrobial effect of nanocomposites and composite based on poly(butylene adipate-co-terephthalate) using Cu and Cu/Cu2O nanoparticles and CuSO4, Nanoscale Res. Lett. 14 (2019), https://doi.org/10.1186/s11671-019-2987-x.
[59] Y. Liu, X. Shao, J. Huang, H. Li, Flame sprayed environmentally friendly high density polyethylene (HDPE)– capsaicin composite coatings for marine antifouling applications, Mater. Lett. 238 (2019) 46–50, https://doi.org/10.1016/j.matlet.2018.11.144.
[60] A.-T. Periferakis, A. Periferakis, K. Periferakis, A. Caruntu, I.A. Badarau, I. Savulescu-Fiedler, C. Scheau, C. Caruntu, Antimicrobial properties of capsaicin: available data and future research perspectives, Nutrients 15 (2023) 4097, https://doi.org/10.3390/nu15194097.
[61] T. Guo, M. Li, X. Sun, Y. Wang, L. Yang, H. Jiao, G. Li, Synergistic activity of capsaicin and colistin against colistin-resistant acinetobacter baumannii: in vitro/vivo efficacy and mode of action, Front. Pharmacol. 12 (2021) 1–14, https://doi.org/10.3389/fphar.2021.744494.